An Adaptive Direct Quadrature Method of Moment for Population Balance Equations

Junwei Su
Dept. of Mechanical Engineering and Automation, Xi'an Jiaotong University, Xi'an 710049, China

Zhaolin Gu
Dept. of Environmental Science and Technology, School of Human Settlements and Civil Engineering, Xi'an Jiaotong University, Xi'an 710049, China

Yun Li and Shiyu Feng
Dept. of Process Equipment and Control Engineering, Xi'an Jiaotong University, Xi'an 710049, China

X. Yun Xu
Dept. of Chemical Engineering and Chemical Technology, Imperial College London, London, UK

DOI 10.1002/aic.11599
Published online September 26, 2008 in Wiley InterScience (www.interscience.wiley.com).

Quadrature method of moments (QMOM) and direct quadrature method of moments (DQMOM) for population balance equations (PBE) have been shown to be accurate and computationally efficient for isotropic systems or when used with computational fluid dynamics (CFD) codes. However, numerical difficulties can arise for cases where there is a large variation of moments or where two abscissas have similar values. Previous study has demonstrated that introducing an appropriate adjustable factor to the QMOM, the numerical difficulty can be alleviated in some cases with an additional benefit of improving numerical accuracy or significantly reducing computational time. However, no reliable method is available to determine the optimal adjustable factor that allows the highest possible accuracy to be obtained while maintaining computational efficiency. In this work, an adjustable factor is introduced to the DQMOM and a novel procedure is proposed that enables the optimal adjustable factor to be found for a given problem. A number of test cases including pure aggregation, pure breakage, pure growth, aggregation and breakage, aggregation and growth have been carried out. Our results show that the proposed method is capable of either improving numerical accuracy or reducing the computational time for a variety of problems. The novelty of this method is that the optimal adjustable factor is determined based on the actual particle size distribution at a given time, thereby reducing error accumulation. It also allows other factor-searching procedures to be incorporated in a straightforward manner without influencing the adaptive DQMOM (ADQMOM)itself. © 2008 American Institute of Chemical Engineers *AIChE J,* 54: 2872–2887, 2008

Keywords: population balance equation, direct quadrature method of moments, dispersed system

Correspondence concerning this article should be addressed to Z. Gu at guzhaoln@mail.xjtu.edu.cn.

Introduction

Dispersed systems are present in many industrial processes. Accurate prediction of the dispersed phase is important for our understanding of the overall behavior of the system concerned. The particle size distribution (PSD) and microbehaviors, such as bubble or droplet breakup and coalescence, of a dispersed phase can alter flow characteristics dramatically. Standard two-fluid models cannot provide detailed information on PSD or microbehaviors. Accurate mathematical models describing phenomena that occur across a wide range of spatial and temporal scales are necessary.

Population balance model is becoming an essential tool for modeling dispersed systems frequently encountered in many engineering applications such as aerosol dynamics, crystallization, precipitation, liquid–liquid, gas–liquid, and combustion process. Population balance equations (PBE) allow us to describe the dispersed phase by means of a number density function (NDF). The evolution of NDF must take into account the different processes controlling NDF such as breakage, coalescence, growth, and nucleation. The PBE, a continuous form of NDF, can describe these microbehaviors. But the resulting form is a nonlinear integral-differential equation, and no general analytical solution is available except for limited simple cases. For most practical problems, only numerical solutions are possible. However, such techniques should be accurate and computationally efficient.

A number of numerical methods have been developed to meet the accuracy requirement, among which are class method (CM),[1–3] Monte Carlo method (MCM),[4,5] and method of moment (MOM).[6–8] In the CM, the continuous size range of the internal coordinate is partitioned into a finite series of contiguous subintervals or bins. Satisfactory accuracy can be achieved if a large number of size groups are used, but at the expense of high computational cost because of the increased number of scalars involved. The number of classes is a potential problem in computational fluid dynamics (CFD) applications, especially when a multifluid flow model is used; also there exist finite domain errors in such a method, hence the CM method is not feasible in practice. MCM is based on the solution of PBE in terms of its stochastic equivalent. A population of particles undergoes realistic physical processes and events occur according to their respective probabilities. A very large number of particles are required to minimize statistical errors. Because of limitations on computational resources, it is still not possible to fully incorporate MCM into a CFD code.[8] Generally, existing nonstochastic numerical methods for PBE can be derived from weighted residual method depending on weight function, trial function, and support domain. For instance, if monomials of 1, x, x^2, x^3,..., x^n are chosen as the weight functions, different MOMs with different trial functions can be derived, e.g. in QMOM,[7] Dirac delta function is adopted in the overall domain. Note that in traditional weighted residual methods, the nodes are fixed throughout the simulation time (e.g., in finite element methods) or updated with their new locations at the end of each time step (e.g., in meshfree methods). But in QMOM, the nodes and their values are allowed to change simultaneously by using special algorithms, such as the product-difference (PD) algorithm[7] or Jacobian matrix transformation (JMT).[9] Thus, high accuracy can be achieved with a small number of nodes, usually three nodes in QMOM.[10] However, with the use of Dirac delta function and limited nodes, detailed information about particle size distribution cannot be obtained.

With relative high accuracy and low computational cost, QMOM has been widely used[9–13] in the last few years and extended to bivariate cases.[14] However, it is difficult to apply this method to systems where the dispersed-phase velocity is strongly dependent on internal coordinates (e.g., fluidized bed and bubble column), and the method can become quite complex in the case of bivariate PBE.[15] Fan et al. (2004) proposed the direct quadrature method of moment (DQMOM),[8] which can be extended to multivariable applications relatively easily. QMOM and DQMOM are essentially the same in mathematics for constant velocity, monovariate cases.[15] DQMOM allows transport equations for weights and abscissas to be derived without resorting to the PD algorithm. For a homogenous system, JMT can serve this purpose,[9] but it cannot determine how the weights and abscissas change due to spatial transport for inhomogeneous cases, for example as a consequence of the presence of a spatial diffusion term.[15]

Our previous studies have revealed three main problems with the standard DQMOM. (1) The numerical accuracy or computational expense of DQMOM depends strongly on relative magnitude of the moments. If two abscissas have approximately the same values, the matrix in DQMOM would become extremely difficult to solve, resulting in the source term of PBE being too large and negative weights or abscissas appearing in the simulation. (2) If simulations need to be carried out for a long period of time (physical time), numerical errors associated with DQMOM tend to accumulate and even escalate to an unacceptable level. (3) In some cases, the numerical accuracy of DQMOM is highly sensitive to physical parameters. To circumvent these problems, an adjustable factor was introduced into DQMOM as performed by Su et al.[6] for QMOM. Another novelty of this work is that we developed a procedure for obtaining the optimal adjustable factor based on a general rule for the condition number of the matrix constructed in DQMOM. The most appropriate adjustable factor at a given time can be found through such a procedure automatically. A wide range of test cases including aggregation, breakage, growth, and combined processes, aggregation growth, aggregation breakage have been performed to validate this method.

Mathematical models

Population balance model

In a dispersed system, particles are dispersed in a surrounding phase, which we shall refer to as the continuous phase. The particles interact with each other and the continuous phase. Such behavior varies from particle to particle depending on both the internal and external states of the particles. Generally, the inherent properties of a particle are referred as internal state, and a particle's spatial position and time t are referred to as external state. The distribution of particles in the state space can be described by a number density function (NDF). NDF can be defined in several ways depending on the properties of the system concerned. Given

the coordinates of the state vector (ξ, **x**, t) that represents the state of the particles, the NDF f (ξ, **x**, t) can be written as[10]

$$f(\xi_1,\ldots,\xi_N;\mathbf{x},t)d\xi_1,\ldots,d\xi_N = f(\xi;\mathbf{x},t)d\xi \tag{1}$$

where $\xi_i (i = 1,\ldots,N)$ represent particle properties, size, or volume, etc. **x** is the spatial location of particle and t is time. Equation 1 represents the number of particles whose property vector has a value between ξ and $\xi + d\xi$ at time t and location **x**. This equation may have different forms depending on the properties concerned. In this work, only the size of particle is of interest. Thus, the property vector ξ becomes a scalar L.

PBE is a continuous form of NDF. The length-based PBE can be expressed as

$$\frac{\partial f(L;\mathbf{x},t)}{\partial t} + \frac{\partial}{\partial x_i}\left(\langle \mathbf{u}_i\rangle_L f(L;\mathbf{x},t)\right) - \frac{\partial}{\partial x_i}\left(D_x \frac{\partial f(L;\mathbf{x},t)}{\partial x_i}\right) = S(L) \tag{2}$$

Equation 2 conforms to the Einstein sum assumption, where f (L; **x**, t) is the number density function; $\langle \boldsymbol{u}_i\rangle_L$ is the particle mean velocity conditioned on property value L at i direction. The diffusion coefficient D_x can be made more general by including anisotropic effects and a dependence on L. $S(L)$ is the source term of PBE, which is related to detailed microbehaviors in a dispersed system. The mathematical expression for $S(L)$ can be in single integral, multiintegral, or differential form with respect to the NDF.

Adjustable moments and quadrature approximation

It is computationally intractable to solve Eq. 2 directly in practical sense. One of the most popular numerical methods is MOM, where the PSD is not tracked directly, but through its moments integrated over the internal coordinate. To adapt the moments according to a certain PSD, we define the adjustable moments below

$$m_k(t) = \int_0^\infty L^{k/p} f(L;t)dL \tag{3}$$

where $m_k(t)$ is an adjustable moment of the PSD; $f(L;\ t)$ is the number density function of characteristic length L, and p is the adjustable factor ($p = 1$ is equivalent to the conventional moments). The adjustable moment m_k has different physical meanings depending on the relation of k and p. When $k = 0$ then $m_0(t)$ is the total number of entities considered; when $k = 2p$, $m_{2p}(t)$ is related to the total area ($A_t = k_A m_{2p}$) of all the entities; and when $k = 3p$, m_{3p} is related to the total volume ($V_t = k_v m_{3p}$). The shape factors k_A and k_v are determined by the entity morphology. The Sauter diameter d_{32} in a polydisperse system can be defined as follows, which is the ratio of total volume and total area.

$$d_{32} = \frac{m_{3p}}{m_{2p}} = \frac{\int_0^\infty f(L;t)L^3 dL}{\int_0^\infty f(L;t)L^2 dL}, \tag{4}$$

If the moment transformation is applied to Eq. 2, it is possible to derive a number of transport equations for mean properties, mass, particle number, and so on. However, a number of unclosed terms arise and much effort has focused on developing closures for these terms. In QMOM and DQMOM, Gaussian quadrature approximation is used to serve this purpose, which assumes NDF to have the form

$$f(L;t) = \sum_{a=1}^{N} \omega_a(t)\delta[L - L_a(t)] \tag{5}$$

where ω_a are weights, L_a are abscissas, $\delta(L)$ is Dirac delta function, N is the total number of quadrature nodes. By using Eq. 5, any integral expression involving NDF can be transformed into a summation.

After adjustable moment transformation using Eqs. 3–5 gives

$$m_k(t) = \sum_{a=1}^{N} \omega_a(t) L_a^{k/p} = \sum_{a=1}^{N} \omega_a(t) l_a^k \tag{6}$$

where $l_a = L_a^{1/p}$, can be regarded as equivalent abscissas which are similar to abscissas in the standard moment. Note that the abscissas are not altered after introducing the adjustable factors, but the equivalent abscissas are different. For example, when $p = 1$, the equivalent abscissas are the particle sizes and when $p = 1/3$ the equivalent abscissas correspond to the volumes. The moments can be obtained once the values for weights ω_a and L_a are found.

It is worth pointing out that the definition of adjustable moments, i.e. Eq. 3, does not dictate that the adjustable moments must be fractional moments. In theory, p can take any real values. However, to conserve mass in the simulation of aggregation or breakage processes, values of p have to be chosen from a finite range of {1/3, 2/3, 1, 4/3, 5/3} if three quadrature nodes are adopted. Whereas in growth processes, any real values for p can be used since the 0th moment m_0 is automatically tracked in DQMOM as well as the method presented here.

Adaptive direct quadrature method of moment

The primary difference between DQMOM and the adaptive DQMOM (ADQMOM) proposed here lies in the definition of the moment. Similar to the derivation of DQMOM, Eq. 5 can be substituted into Eq. 2 and after some manipulations, Eq. 2 can be written as follows:

$$\sum_{a=1}^{N}\left[\delta(L-L_a) - \delta'(L-L_a)L_a\right]\phi_a - \sum_{a=1}^{N}\delta'(L-L_a)\varphi_a = \sum_{a=1}^{N}\delta''(L-L_a)C_a + S(L) \tag{7}$$

and,

$$\frac{\partial \omega_a}{\partial t} + \frac{\partial}{\partial x_i}\left(\langle \boldsymbol{u}_i\rangle_a\ \omega_a\right) - \frac{\partial}{\partial x_i}\left(D_x \frac{\partial \omega_a}{x_i}\right) = \phi_a \tag{8}$$

$$\frac{\partial \zeta_a}{\partial t} + \frac{\partial}{\partial x_i}\left(\langle \boldsymbol{u}_i\rangle_a \zeta_a\right) - \frac{\partial}{\partial x_i}\left(D_x \frac{\partial \zeta_a}{x_i}\right) = \varphi_a \tag{9}$$

$$C_a = \omega_a D_x \frac{\partial L_a}{\partial x_i} \frac{\partial L_a}{\partial x_i} \tag{10}$$

where $\langle u_i \rangle_a = \langle u_i \rangle_{L_a}$ is the characteristic velocity associated with the delta function (or dispersed phase a). $\zeta_a = \omega_a L_a$ are weighted abscissas. Detailed derivation of Eq. 7 can be found in Marchisio' work.[15] If the initial values of weights ω_a and abscissas L_a are specified, Eqs. 8 and 9 can be used to determine their values at subsequent time points.

The unknown functions ϕ_a and φ_a are calculated from Eq. 7 by applying the adjustable moment transformation. Applying adjustable moment transformation, Eq. 7 becomes

$$\left(1 - \frac{k}{p}\right) \sum_{a=1}^{N} L_a^{k/p} \phi_a + \frac{k}{p} \sum_{a=1}^{N} L_a^{k/p-1} \varphi_a = \overline{S}_k(t) + \overline{C}_k \tag{11}$$

where the moment source of PBE is determined by

$$\overline{S}_k = \int_0^\infty L^k S(L) dL \tag{12}$$

and

$$\overline{C}_k = p^{-2} k(k-p) \sum_{a=1}^{N} L_a^{k/p-2} C_a. \tag{13}$$

Note that Eq. 11 is a linear system and is used to obtain ϕ_a and φ_a ($a = 0, \ldots, 2N-1$) with $2N$ unknowns. Let $k = 0, \ldots, 2N-1$ denote terms on the right-hand side of Eq. 11 by $\overline{S}_k^{(N)}$, Eq. 11 can be written in matrix form

$$A\alpha = d \tag{14}$$

where,

$$A = [A_1 A_2] \tag{15}$$

$$A_1 = \begin{bmatrix} 1 & \cdots & 1 \\ \frac{p-1}{p} L_1^{\frac{1}{p}} & \cdots & \frac{1}{p} L_N^{\frac{1}{p}} \\ \frac{p-2}{p} L_1^{\frac{2}{p}} & \cdots & \frac{p-2}{p} L_N^{\frac{2}{p}} \\ \vdots & \vdots & \vdots \\ (1 - \frac{2N-1}{p}) L_1^{\frac{2N-1}{p}} & \cdots & (1 - \frac{2N-1}{p}) L_N^{\frac{2N-1}{p}} \end{bmatrix} \tag{16}$$

$$A_2 = \begin{bmatrix} 0 & \cdots & 0 \\ \frac{1}{p} L_1^{\frac{1}{p}-1} & \cdots & \frac{1}{p} L_N^{\frac{1}{p}-1} \\ \frac{2}{p} L_1^{\frac{2}{p}-1} & \cdots & \frac{2}{p} L_N^{\frac{2}{p}-1} \\ \vdots & \vdots & \vdots \\ \frac{2N-1}{p} L_1^{\frac{2N-1}{p}-1} & \cdots & \frac{2N-1}{p} L_N^{\frac{2N-1}{p}-1} \end{bmatrix} \tag{17}$$

$$\alpha = [\phi_1 \cdots \phi_N \quad \varphi_1 \cdots \varphi_N]^T = \begin{bmatrix} \phi \\ \varphi \end{bmatrix} \tag{18}$$

$$d = [\overline{S}_0^{(N)}, \ldots, \overline{S}_{2N-1}^{(N)}] \tag{19}$$

we can obtain α from

$$\alpha = A^{-1} d. \tag{20}$$

For a homogenous system, the second term on the right-hand side of Eq. 11 can be omitted. Hence, we only need to deal with microbehavior induced source terms, i.e. Eq. 12.

Aggregation

A general description of aggregation with respect to length in any system can be expressed as follows,[11] but with different aggregation kernels

$$S(L) = \frac{L^2}{2} \int_0^L \frac{\beta((L^3 - \lambda^3)^{1/3}, \lambda)}{(L^3 - \lambda^3)^{2/3}} f((L^3 - \lambda^3)^{1/3}; t) f(\lambda; t) d\lambda - f(L; t) \int_0^\infty \beta(L, \lambda) f(\lambda; t) d\lambda \tag{21}$$

where $\beta(L, \lambda)$ is the length-based aggregation kernel describing the frequency at which entities with sizes L and λ collide to form a entity of size $(L^3+\lambda^3)^{1/3}$, which is usually written as the product of collision frequency and aggregation efficiency. The first term on the right-hand side is the rate of birth of entities of size L because of the aggregation of smaller entities, whereas the second term on the right-hand side of the equation is the rate of death of entities of size L due to aggregation with other entities.

After adjustable moment transformation, Eq. 21 becomes

$$\overline{S}_k(t) = \frac{1}{2} \int_0^\infty f(\lambda; t) \int_0^\infty \beta(L, \lambda) (L^3 + \lambda^3)^{\frac{k}{3p}} f(L; t) dL d\lambda - \int_0^\infty L^{\frac{k}{p}} f(L; t) \int_0^\infty \beta(L, \lambda) f(\lambda; t) d\lambda dL \tag{22}$$

Applying Gaussian quadrature approximation gives

$$\overline{S}_k(t) = \frac{1}{2} \sum_{i=1}^{N} \sum_{j=1}^{N} \omega_i \omega_j (L_i^3 + L_j^3)^{\frac{k}{3p}} \beta_{ij} - \sum_{i=1}^{N} \sum_{j=1}^{N} \omega_i \omega_j L_i^{\frac{k}{p}} \beta_{ij} \tag{23}$$

where $\beta_{ij} = \beta(L_i, L_j)$. Note that mass conversation in the aggregation process without entities' removal requires $k = 3p$. For a quadrature approximation with three nodes, the adjustable factor p should be in the range of $\{1/3, 2/3, 1, 4/3, 5/3\}$.

Breakage

A general description of the breakage process can be written as follows[11]

$$S(L) = \int_L^\infty a(\lambda) b(L|\lambda) d\lambda - a(L) f(L; t) \tag{24}$$

where $a(L)$ is the breakage kernel, which depends on characteristics of particles and the surrounding fluid; $b(L|\lambda)$ is the daughter distribution depending on the vortex intensity or thermal stress. The first and second terms on the right-hand side of Eq. 24 are, respectively, the birth and death rates of entities of size L due to fragmentation.

After adjustable moment transformation, Eq. 24 becomes

$$\overline{S}_k(t) = \int_0^\infty L^{\frac{k}{p}} \int_0^\infty a(\lambda) b(L|\lambda) f(\lambda; t) d\lambda dL - \int_0^\infty L^{\frac{k}{p}} a(L) f(L; t) dL. \tag{25}$$

Applying Gaussian quadrature approximation yields

$$\overline{S}_k(t) = \sum_{i=1}^{N} a_i \overline{b}_i^{(k)} \omega_i - \sum_{i=1}^{N} L_i^{\frac{k}{p}} a_i \omega_i \tag{26}$$

with

$$a_i = a(L_i) \tag{27}$$

$$\overline{b}_i^{(k)} = \int_0^\infty L^{\frac{k}{p}} b(L|L_i) dL. \tag{28}$$

Note that $k = 3p$ is required to ensure mass conversation in the breakage process. If the quadrature approximation with three nodes is adopted, the adjustable factor should be in the range of {1/3, 2/3, 1, 4/3, 5/3}.

Growth

Particle growth can be described as follows using different growth rates[15]

$$S_L(L) = -\frac{\partial}{\partial L}[G(L)n(L)]. \tag{29}$$

Applying the adjustable moment transformation, Eq. 29 becomes

$$\overline{S}_k(t) = \frac{k}{p}\int_0^\infty G(L)f(L;t)L^{\frac{k}{p}-1} dL. \tag{30}$$

Applying the quadrature approximation, we obtain

$$\overline{S}_k(t) = \frac{k}{p}\sum_{i=1}^{N} \omega_i G(L_i) L_i^{\frac{k}{p}-1}. \tag{31}$$

It should be noted that, for pure growth processes without any particle removal, the total number of particles should remain constant. Therefore, $k = 0$ and the particle number is automatically tracked. Thus, there is no constraint in the selection of adjustable factors.

It is worth noting that the method proposed here is not a general form for different internal coordinates. ADQMOM allows different moments to be tracked by using different adjustable factors. For example, when $p = 1/3$, the moments of entity volume $(L^3)^k$ can be tracked but the internal coordinate is always length. The relationships between the moments and the internal coordinate are different in ADQMOM and QMOM.

Determination of optimal adjustable factor

In aggregation or breakage processes, the values of adjustable factor are restricted, whereas in growth process the values can be arbitrary. To obtain a more appropriate adjustable factor, we should analyze the sources of numerical errors. There are two primary potential sources of numerical error in DQMOM, those originating from numerical integration of ordinary differential equation (ODE) and from matrix inversion (see Eq. 20). The errors introduced by integration of ODE can be enormous depending largely on the method employed and the problem concerned. We carried out a number of test cases using different integration methods: Runge-Kutta method with changing step and error monitoring, Runge-Kutta method with adaptive time step and error monitoring, and Gill method with changing step and error monitoring. Among these integration methods, it seemed that Gill ODE integration method with changing step and error monitoring allowed DQMOM and AQMOM to yield the highest accuracy with the same error allowance, so this method was adopted in this work. To handle the data more efficiently, the standard Gill ODE integration method was modified by specifying a fixed time step. If the desired numerical accuracy is achieved with the fixed time step, this time step is adopted, otherwise, the fixed time step will be divided into a number of uniform steps, and integration will be carried out over smaller steps to obtain the desired accuracy. Since the error resulted from ODE integration can be controlled by error monitor, the attention was turned to reducing errors from matrix inversion. Because of the relatively low rank of the matrix, convectional matrix inversion procedure can be used, such as Gauss-Jordan elimination method. The values in the constructed matrix could vary considerably depending on the inherent property, which makes the matrix ill-conditioned. Matrix inversion tends to introduce large errors for an ill-conditioned matrix, and thus we investigated the condition number of the matrix constructed in DQMOM.

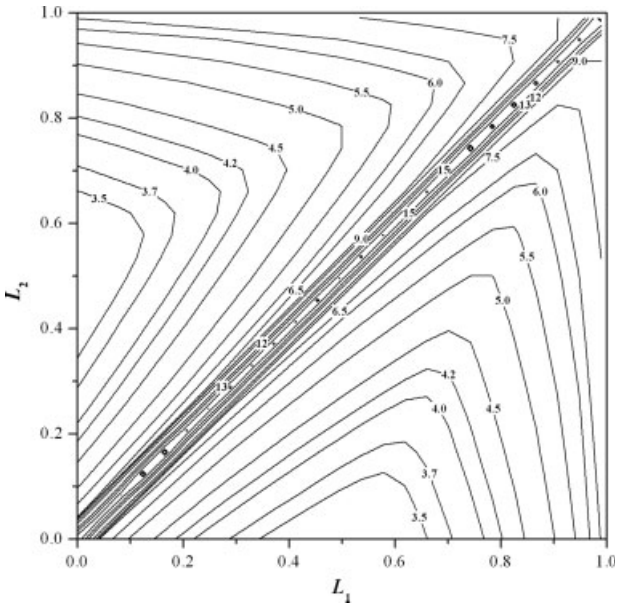

Figure 1. Logarithm distribution of condition number.

In the DQMOM and QMOM, three quadrature nodes are usually adopted. If L_1, L_2, and L_3 denote the three abscissas and $L_3 = \max(L_1, L_2, L_3)$, the abscissas can be normalized by $L_i = L_i/L_3$ ($i = 1, 2, 3$), hence $L_1, L_2 \in (0, 1)$, and $L_3 = 1$. Let L_1 and L_2 vary between 0 and 1, and construct the matrix $\boldsymbol{A}$ with $p = 1$ in Eq. 15 using Eqs. 16 and 17, the condition number can be calculated using

$$\text{Cond }(\boldsymbol{A}) = ||\boldsymbol{A}^{-1}||\,||\boldsymbol{A}|| \tag{32}$$

where, $\|\boldsymbol{A}\|$ is the norm of matrix $\boldsymbol{A}$.

Figure 1 shows the logarithmic distribution of condition number. It is clear that if any two of the three abscissas have approximately the same value, the condition number would become very large. The more uniform the distribution of the abscissas, the smaller the condition number and the higher the numerical accuracy in the matrix inversion.

Previous studies showed that the numerical problems encountered in DQMOM or QMOM were mainly caused by

the large divergence among the weights and nonuniformity of the abscissas. After introducing an adjustable factor, the relative magnitude of equivalent abscissas can be changed so that their distribution becomes more uniform. It was also found that a uniform distribution of the values of the abscissas gave larger standard derivation of the abscissas. Therefore, it is possible to find the optimal adjustable factor with which the equivalent abscissas have the largest standard deviation. Also, the equivalent abscissas with different adjustable factors are normalized before calculating the standard derivation to ensure that they correspond to the same position. A numerical procedure was implemented to determine the optimal adjustable factor for breakage and aggregation processes, and this is described as follows.

(1) Choose adjustable factors $p_j (j = 1,\ldots,2N - 1)$ and calculate equivalent abscissas

$$l_i = L_i^{1/p_i} \quad i = 1,\ldots,N \tag{33}$$

(2) Normalize the equivalent abscissas

$$l_i = l_i / \max(l_1, l_2, \ldots, l_N) \tag{34}$$

(3) Calculate the standard deviation

$$s_j = \left(\frac{1}{N-1} \sum_{i=1}^{N} (l_i - \bar{l})^2 \right)^{1/2} \tag{35}$$

where,

$$\bar{l} = \frac{1}{N} \sum_{i=1}^{N} l_i \tag{36}$$

(4) Find the index j corresponding to the maximum s_j, and then p_j.

For a growth process, the adjustable factor p can take any arbitrary values. One can find the maximum value of s in Eq. 35 with respect to p, and find the value of p with which Eq. 35 reaches the maximum. Since the procedure for finding the maximum s can be computationally intensive and a very small p could result in excessively high computational expense, it would be desirable to artificially restrict the values for p within a finite range, as performed by Su et al.[6]

The procedure for determining the optimal adjust factor is carried out at each time step based on instantaneous values of the equivalent abscissas. Note that all mathematical manipulations of the abscissas, such as adjustment using Eq. 33 and normalization using Eq. 34, will not affect their actual values as they are only carried out for searching the optimal factor.

Test cases

All the test cases in this work were carried out on a desktop PC with Intel 1.8 GHZ, 512 MB memory. The quadrature approximation with three nodes was adopted. To compare numerical predictions with analytical solutions, the abscissas and weights were converted to the length-based moments using Eq. 6 with $p = 1$. Coupling of this procedure with CFD is beyond the scope of this work, but will be attempted in a future study.

Pure aggregation

Four test cases were carried out to validate the present method for pure aggregation. For the first test case, a constant aggregation kernel was adopted, i.e.

$$\beta(L, \lambda) = C_0 \tag{37}$$

with $C_0 = 1$, and the exponential initial particle distribution

$$f(L) = \frac{3N_0}{V_0} L^2 \exp\left(-\frac{L^3}{V_0} \right) \tag{38}$$

where $N_0 = 1$ and $V_0 = 1$. In this case, the analytical solution for the moment for the adjustable factor $p = 1$ was given by[10]

$$m_k(t,\ p=1) = m_k(t=0,\ p=1) \left(\frac{2}{2 + N_0 C_0 t} \right)^{1-k/3}. \tag{39}$$

Differences between the predicted moments and the analytical solution were evaluated and the variations of percent errors (relative to the analytical solution) with time are shown in Figure 2 for (a) DQMOM and (b) ADQMOM. Errors for m_3 for both methods were below 10^{-12}%, hence are not included in the figure. With ADQMOM, relative errors for m_1 and m_5 differed very little, and similar observations were made for m_2 and m_4. It can be seen that the maximum error for all the moments in standard DQMOM is 0.58%, and there is little difference among errors for m_1, m_2, m_4 and m_5, whereas with ADQMOM, errors for all the moments are below 10^{-10}%. Both the methods yielded accurate results for m_0 and achieved a similar order of accuracy. By introducing the optimal adjustable factor, numerical errors for all moments except m_0 and m_3 were reduced significantly.

For a time step of 0.01 s and a total simulation time (physical time) of 50 s, the computational time was 13,910 ms for the standard DQMOM and 13,640 ms for ADQMOM, a marginal saving after introducing the optimal adjust factor.

In the second test case for pure aggregation, the same constant aggregation kernel, i.e., Eq. 37, was adopted but with a Gaussian-like initial distribution

$$f(L) = 3L^5 \frac{N_0}{V_0^2} \exp\left(-\frac{L^3}{V_0} \right) \tag{40}$$

with parameters $N_0 = 1$ and $V_0 = 1$. For this case, an analytical solution for the NDF is also available[16]

$$f(L;t) = 3L^2 \frac{(1-T)^2}{T^{1/2}} \frac{N_0}{V_0} \exp\left(-\frac{L^3}{V_0} \right) \sinh\left(\frac{L^3}{V_0} T^{1/2} \right) \tag{41}$$

where,

$$T = \frac{C_0 N_0 t}{2 + C_0 N_0 t}. \tag{42}$$

The standard moments for Eq. 41 can be obtained numerically by solving Eq. 3 with $p = 1$. Percentage errors for the moments are shown in Figure 3 for the standard DQMOM and ADQMOM. Again, the errors for m_3 are below 10^{-12}%,

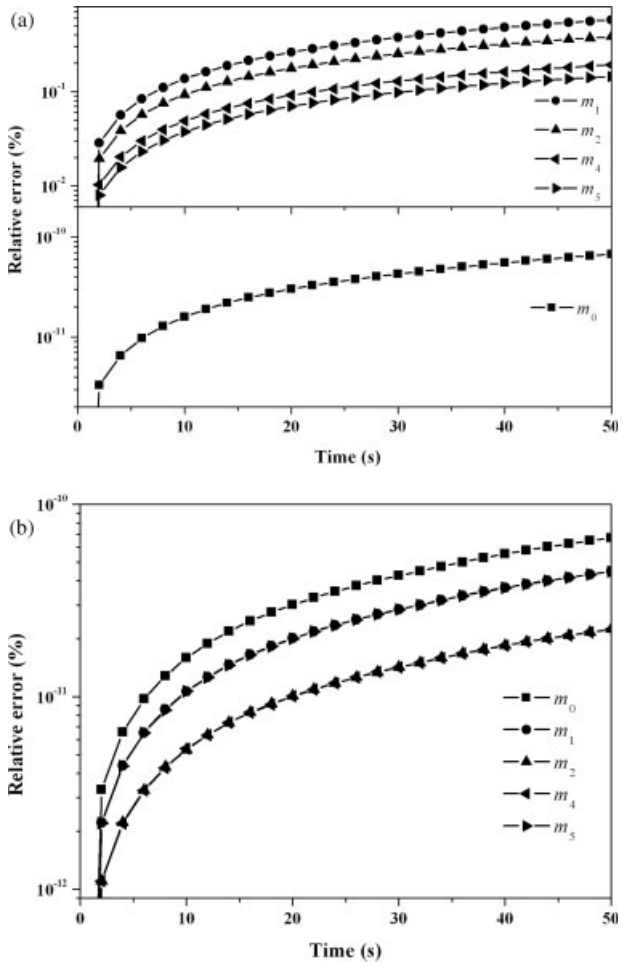

Figure 2. Evolution of percentage errors with time for the first six moments using DQMOM and ADQMOM for aggregation with a constant kernel and exponential initial distribution.

"Square": m_0, "Circle": m_1, "Up triangle": m_2, "Left triangle": m_4, "Right triangle": m_5. (a) DQMOM, (b) ADQMOM.

hence are not included in the figures. With DQMOM, the maximum error is 0.38%, but with ADQMOM errors for all the moments are below 10^{-10}%. Both methods are able to predict the particle number evolution (i.e. the 0th moment m_0) accurately.

With a time step 0.01 s and a simulation time (physical time) of 50 s, the computational time was 103,168 ms for DQMOM and 109,507 ms for ADQMOM. In this case, ADQMOM is capable of dramatically improving the numerical accuracy at very little additional computational expense.

In the third test case, a sum kernel was adopted,

$$\beta(L,\lambda) = C_0(L^3 + \lambda^3) \tag{43}$$

where $C_0 = 0.01$, and the initial distribution was exponential, i.e. Eq. 38. An analytical solution for NDF was given by[16]

$$f(L;t) = \frac{3V_0(1-T)\exp(-L^3(1+T)/V_0)}{LT^{1/2}} I_1(2L^3T^{1/2}/V_0) \tag{44}$$

where $T = 1-\exp(-C_0N_0V_0t)$, $I_1(x)$ is the modified Bessel function of the first kind. Numerical integration was performed to obtain the standard moments.

Percentage errors for all the moments are shown in Figure 4 for (a) DQMOM and (b) ADQMOM. It can be observed that errors for the moments using ADQMOM do not seem to follow any particular pattern. This is caused by the combined influence of the errors due to integration when evaluating the moments and the errors of the method itself. However, this is not the case with DQMOM, since the errors from DQMOM is much larger than those involved in evaluating the standard moments from the analytical solution of NDF. The maximum relative error for all the moments with DQMOM is 3.97%, whereas all the relative errors for the new method are below 10^{-5}%. Note that even though mass conservation was considered in the simulation, errors for m_3, which should have reached the computer accuracy, are larger than 10^{-12}% with both methods due to integration errors when evaluating the standard moments. Both the methods can predict m_0 and m_3 accurately.

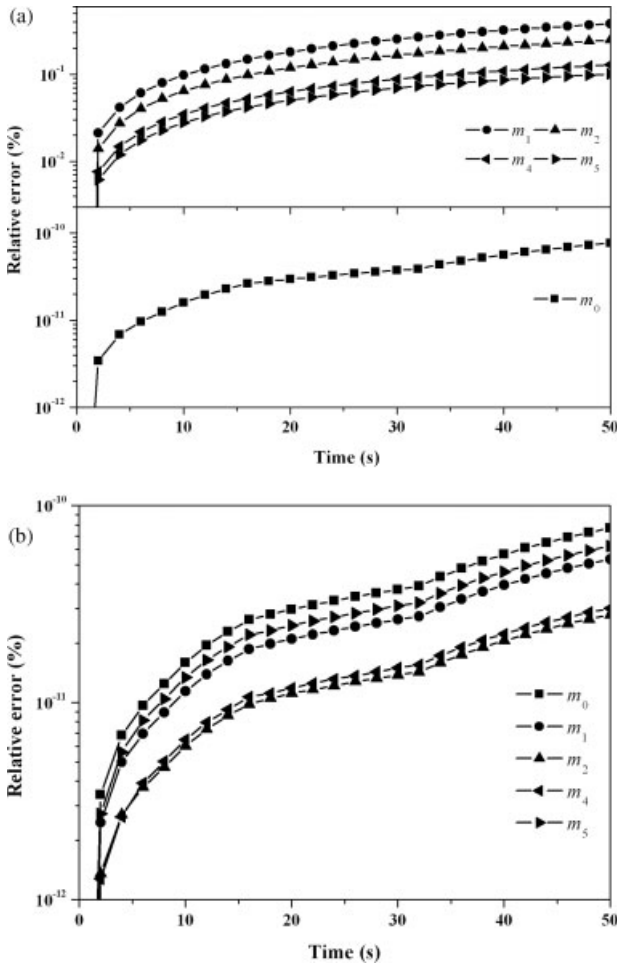

Figure 3. Evolution of percentage errors with time for the first six moments using DQMOM and ADQMOM for aggregation with a constant kernel and Gaussian-like initial distribution.

"Square": m_0, "Circle": m_1, "Up triangle": m_2, "Left triangle": m_4, "Right triangle": m_5. (a) DQMOM and (b) ADQMOM.

With a time step 0.01 s and a simulation time (physical time) of 50 s, the computational time was 288,214 ms for DQMOM and 302,304 ms for ADQMOM. Similar to the previous test case, ADQMOM has dramatically improved the numerical accuracy without incurring too much additional computational cost.

In the fourth test case, a product aggregation kernel was adopted having the form

$$\beta(L,\lambda) = C_0 L^3 \lambda^3 \tag{45}$$

where $C_0 = 0.01$. An exponential initial particle distribution (Eq. 38) with $N_0 = 1$ and $V_0 = 1$ was applied. In such a case, analytical solution was given by[16]

$$f(L;T) = \frac{3N_0L^2}{V_0^{3k+1}} \exp\left(-L^3(1+T)/V_0\right) \sum_{k=0}^{\infty} \frac{T^k L^{9k}}{(k+1)!\Gamma(2k+2)} \tag{46}$$

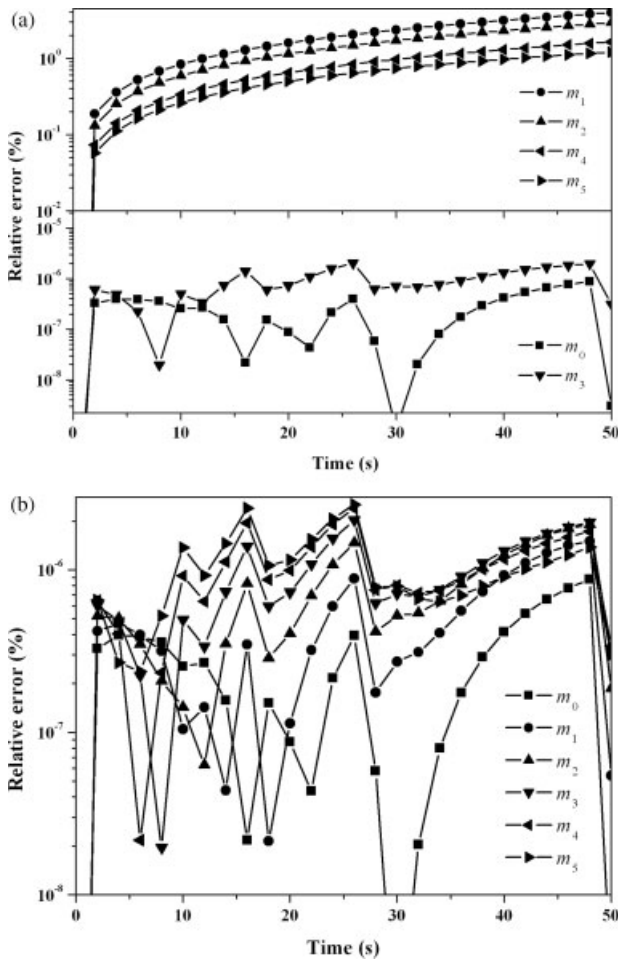

Figure 4. Evolution of percentage errors with time for the first six moments using DQMOM and ADQMOM for aggregation with a sum kernel and exponential initial distribution.

"Square": m_0, "Circle": m_1, "Up triangle": m_2, "Left triangle": m_4, "Right triangle": m_5. (a) DQMOM and, (b) ADQMOM.

Table 1. Exact Moments for the Product Aggregation Kernel

Moments	Analytical Solution
m_0	$m_0(0) - \frac{1}{2}C_0 m_{3p}^2 t,\ 0 < t < t_{\text{gel}}$
m_{3p}	$m_{3p}(0),\ 0 < t < t_{\text{gel}}$
m_{6p}	$m_{6p}(0)/(1-C_0 m_{6p}(0)t),\ 0 < t < t_{\text{gel}}$

where, $T = N_0 C_0 V_0^2 t$ and Γ is the gamma function. Note that the product kernel is a gelling kernel for any initial distribution,[17] so the simulation was carried out before the gelling time t_{gel} started. The analytical solutions for the moment m_0, m_{3p}, and m_{6p} are given in Table 1. Based on the solution for m_{6p}, the actual value for t_{gel} can be calculated

$$t_{gel} = \frac{1}{C_0 m_{6\,p}(0)}. \tag{47}$$

The gelling time t_{gel} was 50 s in this test case. Percentage differences between the numerical results and the analytical solution are presented in Figure 5 for (a) standard DQMOM and (b) ADQMOM. Errors for m_{3p} are less than 10^{-13}% for both the methods, hence are not presented. It is clear that both the methods can predict m_0 accurately, but for the second volume moments m_{6p}, the maximum error is 6.32% with the standard DQMOM, whereas with ADQMOM all the errors are below 10^{-8}%. The computational time was 44,641 ms with DQMOM and 45,969 ms with ADQMOM, showing a negligible increase in computational cost with the new method.

Pure breakage

Three test cases were carried out, one using a constant kernel and the others using power kernels. For a constant kernel

$$a(L) = C_0 \tag{48}$$

with $C_0 = 0.01$ and a uniform daughter distribution

$$b(L|\lambda) = 6\lambda^2/L^3 \tag{49}$$

substituting Eq. 49 into Eq. 28 gives

$$\overline{b}_a{}^{(k)} = \frac{6p}{k+3p} \lambda^{k/p}. \tag{50}$$

Using Eq. 38 as initial distribution, an analytical solution is available for moments with $p = 1/3$[18]

$$m_k(t, p = 1/3) = m_k(t = 0, p = 1/3) \exp\left[\frac{1-k}{1+k} C_0 t\right] \tag{51}$$

To compare the numerical prediction with analytical solution, we can convert the analytical moment of volume (obtained from Eq. 51) to the length-based moment using product-difference (PD) algorithm by the following three steps as performed by Su et al.[6] (1) Solve Eq. 6 to obtain the weights ω_a and equivalent abscissas l_a using PD algorithm; (2) Using the relationship of $L_a = l_a^p$ to get the values of the abscissas L_a with $p = 1/3$; (3) Compute the length-based moment using Eq. 6 with $p = 1$. We can also directly convert the abscissas and weights to moments of volume with $p = 1/3$ and com-

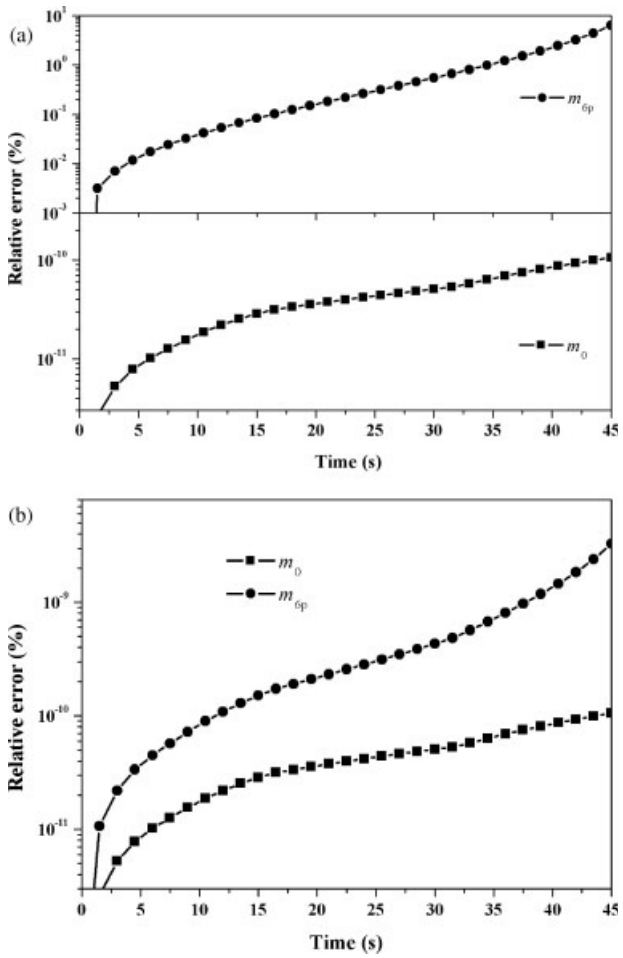

Figure 5. Evolution of percentage errors with time for moments m_0, m_{6p}, before gelling for aggregation with a product kernel and exponent initial distribution.

"Square": m_0, "Circle": m_{6p} (a) DQMOM and (b) ADQMOM.

pare them with the analytical solution (Eq. 51). For consistency, the first method was used. Percentage errors for all the moments (except for m_3 which are below $10^{-12}\%$) are shown in Figure 6 for (a) DQMOM and (b) ADQMOM. It shows that similar level of accuracy is achieved for m_0 and m_3 with both methods, but for the other moments ADQMOM offers far superior accuracy than DQMOM. The maximum error is 4.18% with DQMOM, but below $10^{-9}\%$ with ADQMOM. Again, little additional computational time is needed with the adaptive method. It is also worth mentioning that in this case, the numerical accuracy of DQMOM is rather sensitive to the value for C_0. If $C_0 = 0.1$, the maximum error for all the moments would rise to 53.2%, whereas with ADQMOM all errors would be below $10^{-9}\%$.

In the second test case, a power kernel was selected which has the form

$$a(L) = C_0 L^3 \tag{52}$$

with $C_0 = 0.01$, together with a uniform daughter distribution (Eq. 49) and a power initial distribution (Eq. 38). For this case, the analytical solution for NDF was given by[18]

$$f(L;t) = 3L^2 \frac{N_0}{V_0}(1 + C_0 V_0 t)^2 \exp\left(-\frac{L^3}{V_0}(1 + C_0 V_0 t)\right) \tag{53}$$

The standard moments can be obtained using numerical integration. Percentage errors are shown in Figure 7 for (a) DQMOM and (b) ADQMOM. For this case, there is no great improvement in numerical accuracy with ADQMOM. By performing simulations using different adjustable factors {1/3, 2/3, 4/3, 5/3}, it has also been found that numerical accuracy is insensitive to the choice of adjustable factor as is the case with the QMOM.[6] With a time step 0.01 s and a physical time of 50 s, the computational time was 46,747 ms with DQMOM, but reduced to 20,980 ms with ADQMOM. For this case, the use of an optimal adjustable factor failed to improve numerical accuracy dramatically but reduced the computational time by half when compared with the standard DQMOM.

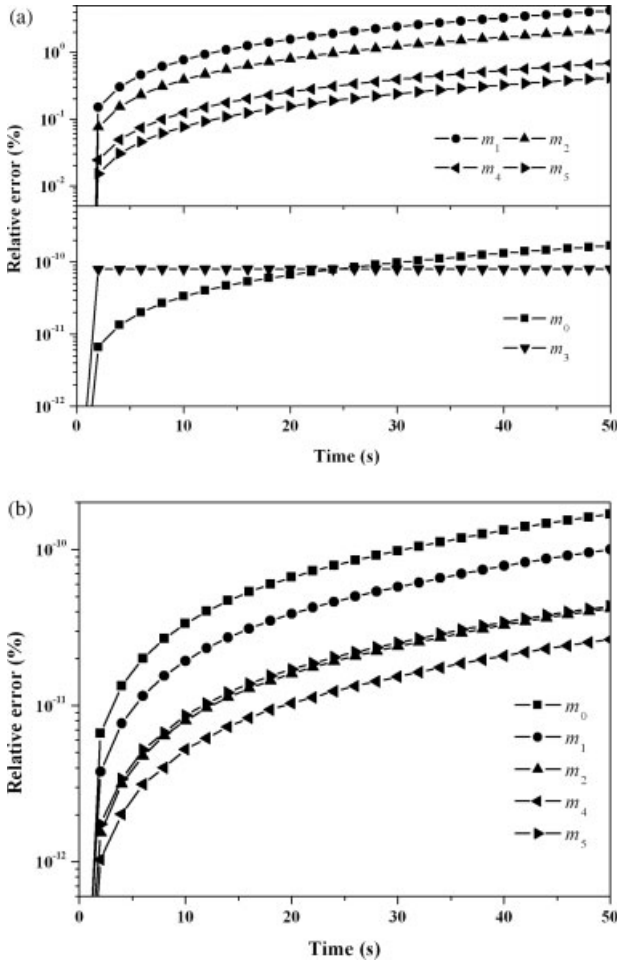

Figure 6. Evolution of percentage errors with time for the first six moments using DQMOM and ADQMOM for aggregation with a sum kernel and exponential initial distribution.

"Square": m_0, "Circle": m_1, "Up triangle": m_2, "Down triangle": m_3, "Left triangle": m_4, "Right triangle": m_5. (a) DQMOM and (b) ADQMOM.

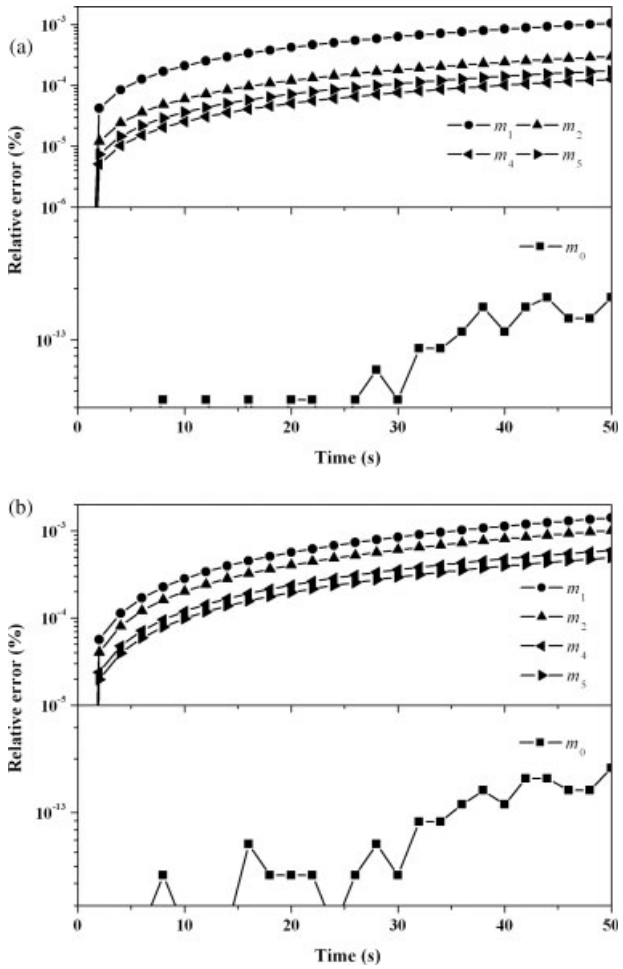

Figure 7. Evolution of percentage errors with time for the first six moments using DQMOM and ADQMOM for breakage with a power kernel C_0L^3 and exponential initial distribution.

"Square": m_0, "Circle": m_1, "Up triangle": m_2, "Down triangle": m_3, "Left triangle": m_4, "Right triangle": m_5. (a) DQMOM and (b) ADQMOM.

In the third test case, a different power kernel was used,

$$a(L) = C_0L^6 \tag{54}$$

with $C_0 = 0.01$. For a uniform daughter distribution and an initial distribution of

$$f(L) = 3L^2\exp(-L^3) \tag{55}$$

an analytical solution can be found[18]

$$f(L;t) = 3L^2[1 + 2C_0t(1 + L^3)]\exp(-C_0L^6t - L^3). \tag{56}$$

Percentage errors for all the moments (except for m_3 which are less than 10^{-12}%) are shown in Figure 8 for (a) DQMOM and (b) ADQMOM. Similar to the previous case, the introduction of an adaptive adjustable factor does not improve the numerical accuracy which is rather insensitive to the choice of adjustable factor. With a time step 0.01 s and a physical time of 50 s, the computational time was 185,847 ms with DQMOM and 181,321 ms with ADQMOM, indicating a small reduction with the latter.

Aggregation and breakage

Two test cases were carried out for such a combined process, where the resulting source term for population balance model is the summation of Eqs. 21 and 24. In the first test case, a constant kernel was used for aggregation (Eq. 37 with $C_0 = 1$), with a Power kernel for breakage, i.e.

$$a(L) = a_0L^3 \tag{57}$$

where $a_0 = 1$. For a uniform daughter distribution and an initial distribution of

$$f(L) = 3\frac{N_0^2}{V_0}L^2\exp\left(-\frac{N_0}{V_0}L^3\right) \tag{58}$$

with $N_0 = 1$ and $V_0 = 10^{-3}$, the analytical solution for NDF can be expressed as[19]

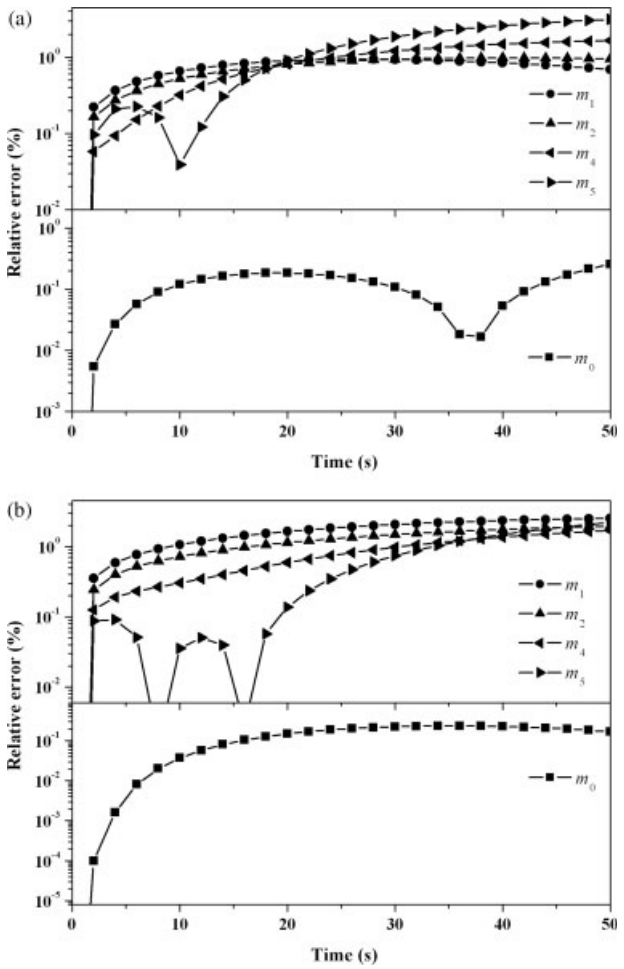

Figure 8. Evolution of percentage errors with time for the first six moments using DQMOM and ADQMOM for breakage with a power kernel C_0L^6 and exponential initial distribution.

"Square": m_0, "Circle": m_1, "Up triangle": m_2, "Down triangle": m_3, "Left triangle": m_4, "Right triangle": m_5. (a) DQMOM and (b) ADQMOM.

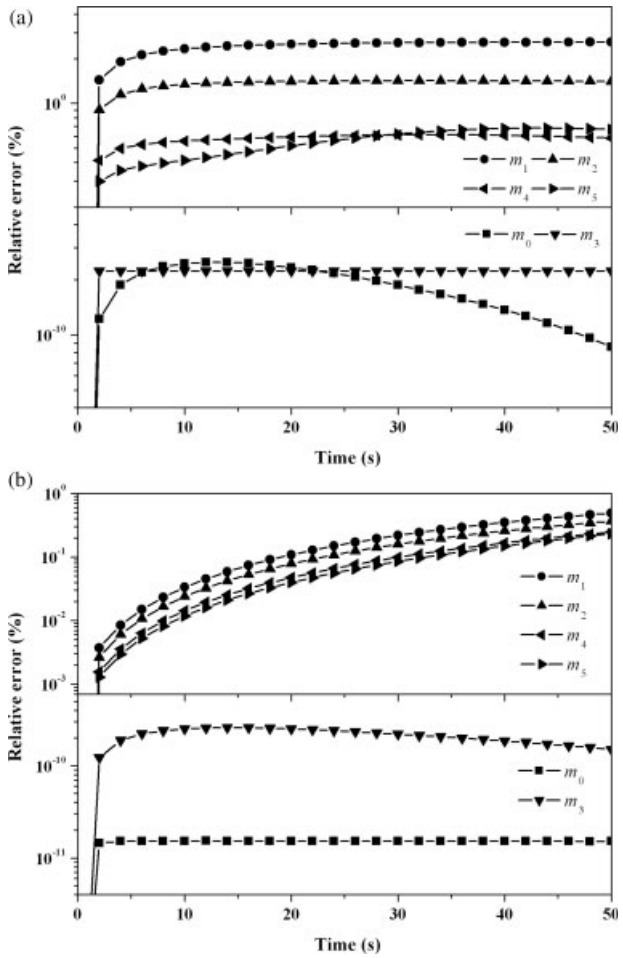

Figure 9. Evolution of percentage errors with time for the first six moments using DQMOM and ADQMOM for aggregation and breakage process.

"Square": m_0, "Circle": m_1, "Up triangle": m_2, "Down triangle": m_3, "Left triangle": m_4, "Right triangle": m_5. (a) DQMOM and (b) ADQMOM.

$$f(L;t) = 3L^2 \frac{N_0^2}{V_0}[\Phi(\tau)]^2 \exp\left[-\frac{N_0}{V_0}L^3\Phi(\tau)\right] \tag{59}$$

where, $\Phi(\tau) = \Phi(\infty)[1 + \Phi(\infty)\tanh(\Phi(\infty)\ \tau/2)]/[\Phi(\infty) + \tanh(\Phi(\infty)\ \tau/2)]$, $\Phi(\infty) = (2a_0V_0/C_0)^{1/2}/N_0$, $\tau = C_0N_0t$. Numerical integration was required to obtain the moments. Percentage errors for the moments are shown in Figure 9 for (a) DQMOM and (b) ADQMOM. It can be observed that numerical accuracy for all the moments has been improved. The maximum error is 2.59% with DQMOM, but less than 1% with ADQMOM. Moreover, there seems to be smaller differences between errors for different moments with the adaptive method. With the standard DQMOM, the error for m_0 reduced with time, whereas with ADQMOM it remained almost constant. The difference in computational time between the two methods is negligible.

In the second test case, the hydrodynamic kernel was used for aggregation, i.e.

$$\beta(L,\lambda) = (L+\lambda)^3 \tag{60}$$

and the breakage kernel had the exponential form

$$a(L) = \begin{cases} 0 & L = 1 \\ 0.1\exp(0.01L^3) & L > 1 \end{cases}. \tag{61}$$

For a uniform daughter distribution and initial moments of $m_k(t = 0;\ p = 1) = \{0.301,\ 0.308,\ 0.372,\ 0.930,\ 5.912,\ 51.0\}$, CM exact solution was available for d_{43} and m_0[11]. A physical time of 50 s was required for a steady state to be reached. Comparison of results obtained from DQMOM, ADQMOM, and the CM exact solution is given in Table 2. It is clear that ADQMOM produced a better accuracy than the standard DQMOM for this case but with a little extra computational load.

Pure growth

Two test cases were carried out. To compare the numerical results from the adaptive method with those of the standard DQMOM and QMOM, the adjustable factor was restricted to the range {1, 2, 3, 4, 5} as done firstly in Su et al.[6]. In the first case, a constant rate was adopted for growth, i.e.

$$G = C_0 \tag{62}$$

with $C_0 = 0.1$. For pure growth without particle removal, the analytical solution was given by[6]

$$m_k(t;\ p=1) = \sum_{i=0}^{k} C_k^i (G_0 t)^i m_{(k-i)}(t=0;\ p=1) \tag{63}$$

where

$$C_k^i = \frac{k!}{(k-i)!i!} \tag{64}$$

with the same initial distribution as in the previous case. It is interesting to note that throughout the simulation time, the value of the adaptive adjustable factor is 1, implying that DQMOM would give the best accuracy if the adjustable factor is artificially restricted to a finite range {1, 2, 3, 4, 5}. The modified QMOM also yielded the best accuracy with an adjustable factor 1 compared with others in the same range.[6] Percentage errors for this case are presented in Figure 10a, where errors for m_0 are very small hence not included.

For growth processes, the adjustable factor can take any real values. Another finite range of {1/3, 2/3, 1, 4/3, 5/3}, which is a necessary condition for aggregation or breakage processes, was also tested using the new adaptive procedure. Percentage errors for all the moments except m_0 for their lower values are given in Figure 10b. It can be observed that

Table 2. Comparison of Computational Time and Results for m_0 and d_{43} Using Different Adjustable Factors and the Exact Solutions Using CM for Aggregation and Breakage

	d_{43}	m_0	Error (m_0) %	Error (d_{43}) %	Time (ms)
DQMOM	0.0179	6.42	1.70	1.38	72,584
CM exact solution	0.0176	6.51			
ADQMOM	0.0174	6.52	1.14	0.15	75,364

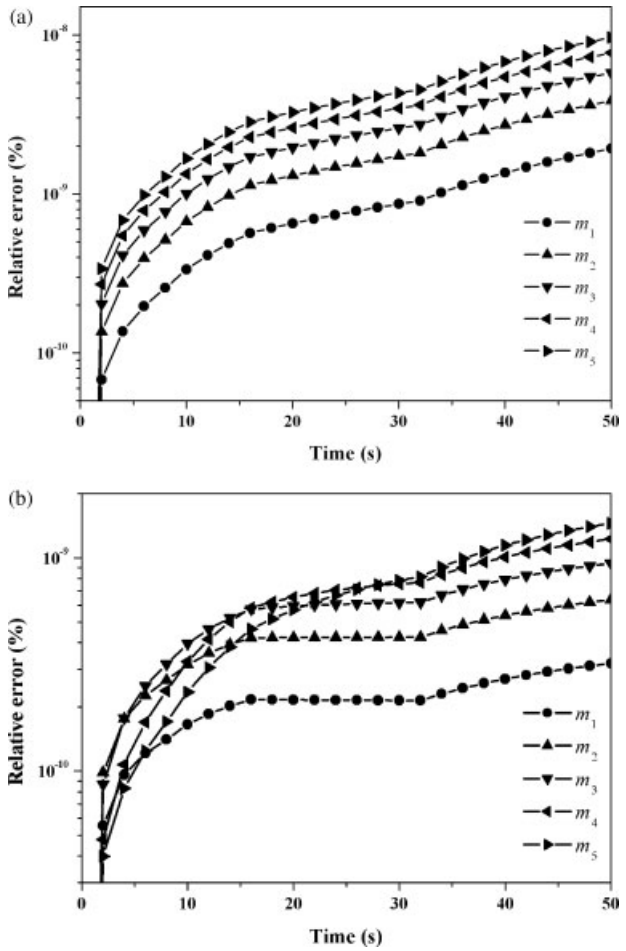

Figure 10. Evolution of percentage errors with time for the first six moments for pure growth with a constant rate.

"Square": m_0, "Circle": m_1, "Up triangle": m_2, "Down triangle": m_3, "Left triangle": m_4, "Right triangle": m_5. (a) DQMOM (ADQMOM with $p = 1$) and (b) ADQMOM.

the maximum error is $1.45 \times 10^{-9}\%$ with ADQMOM, whereas the maximum error is $9.63 \times 10^{-9}\%$ with the standard DQMOM. The difference in computational time between the two test cases is negligible.

In the second test for pure growth, a linear rate was adopted, i.e.

$$G(L) = C_0 L \tag{65}$$

with $C_0 = 0.01$. For such a case, an analytical solution is available[6]

$$m_k(t) = m_k(0)\exp(kG_0 t/p) \tag{66}$$

For the same initial distribution as in the previous case, again with $p = 1$, DQMOM yielded the best accuracy. Percentage errors for this case are plotted in Figure 11a. Similar to the previous case, another finite range of {1/3, 2/3, 1, 4/3, 5/3} for the adjustable factor was adopted. Percentage errors for the moments are shown in Figure 11 for (a) DQMOM (ADQMOM with $p = 1$) and (b) ADQMOM. Note that errors for m_0 are lower than $10^{-13}\%$ with ADQMOM, but are up to $1.9\times10^{-10}\%$ with the standard DQMOM. Errors for the other moments are generally below $10^{-9}\%$ using ADQMOM. Although there are momentary drops in errors at around 35 and 45 s with the standard DQMOM as shown in Figure 11a, ADQMOM gives more accurate and consistent results.

Although the standard DQMOM gives sufficient numerical accuracy for growth processes, ADQMOM is capable of improving it further without additional computational expense. Previous studies showed that the main problem with QMOM or DQMOM was the computational load. After introducing an adjustable factor into QMOM for simulation of growth processes, the computational load was greatly reduced.[6] Future development should focus on reducing computational expense of DQMOM for growth process.

Aggregation and growth

Three test cases for these combined processes were performed and the source term for PBE was the summation of

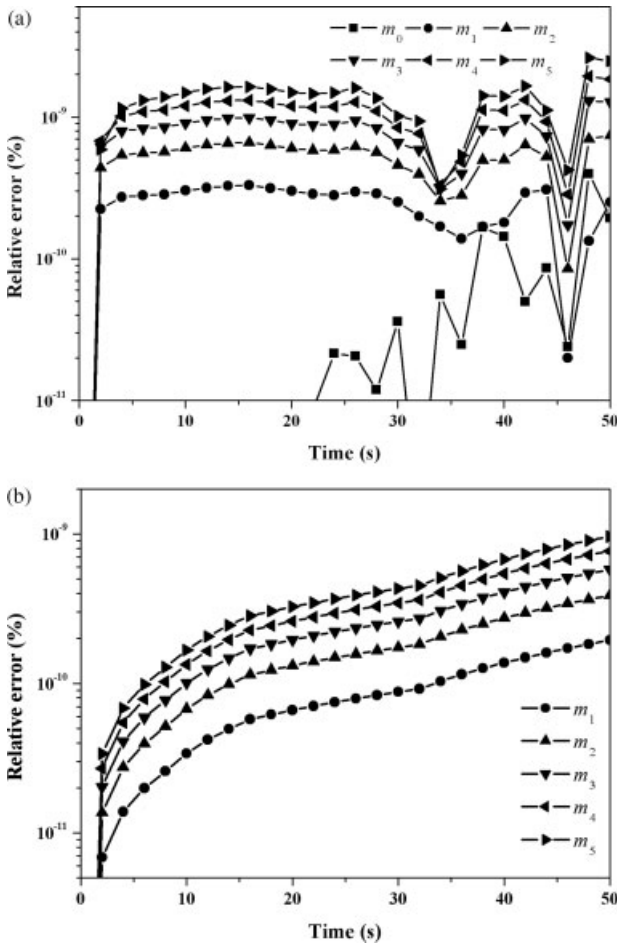

Figure 11. Evolution of percentage errors with time for the first six moments for pure growth with a linear rate.

"Square": m_0, "Circle": m_1, "Up triangle": m_2, "Down triangle": m_3, "Left triangle": m_4, "Right triangle": m_5. (a) DQMOM (ADQMOM with $p = 1$) and (b) ADQMOM.

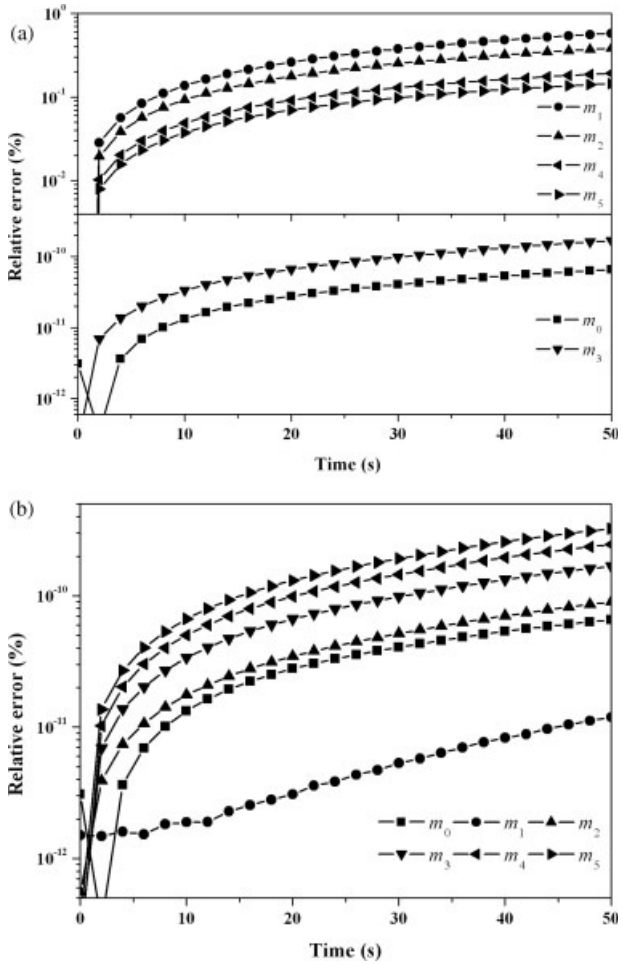

Figure 12. Evolution of percentage errors with time for the first six moments using DQMOM and ADQMOM for aggregation with a constant kernel and growth process with a linear rate together with exponential initial distribution.

"Square": m_0, "Circle": m_1, "Up triangle": m_2, "Down triangle": m_3, "Left triangle": m_4, "Right triangle": m_5. (a) DQMOM and (b) ADQMOM.

Eqs. 21 and 29. Since aggregation behavior was included, the adjustable factor was restricted to {1/3, 2/3, 1, 4/3, 5/3}. In the first case, a constant kernel was used for aggregation, i.e. Eq. 37 with $C_0 = 0.01$, while a linear rate was used for growth, i.e.

$$G(L) = G_0 L/3 \tag{67}$$

with the parameter $G_0 = 0.01$, using Eq. 38 with $N_0 = 1$ and $V_0 = 1$ as the initial distribution. For this case, the analytical solution was given by[20]

$$f(L;t) = 3L^2 \frac{M_0^2}{M_1} \exp\left(-\frac{M_0}{M_1} L^3\right) \tag{68}$$

where $M_0 = 2N_0/(2 + C_0 N_0 t)$, $M_1 = N_0 V_0 \exp(G_0 t)$. The standard moments were obtained by numerical integration. Percentage errors for all the moments are shown in Figure 12 for (a) DQMOM and (b) ADQMOM. The results show that with the standard DQMOM the maximum error for all the moments is 0.57%, whereas with ADQMOM all errors are below 10^{-9}%. Without using an adjustable factor, m_1 has the largest error among all the moments, but with the introduction of an optimal adjustable factor its error becomes the smallest. With a time step of 0.01 s and a physical time of 50 s, the computational time was 187,079 ms with DQMOM and 188,471 ms with ADQMOM.

In the second test case, the same aggregation kernel and growth rate as those in the previous case were used but with a Gauss-like distribution, i.e. Eq. 40. For this case, the analytical solution is also available[20]

$$f(L;t) = 3L^2 \frac{M_0^2}{M_1} \frac{1}{(1 - M_0/N_0)^{1/2}} \exp\left(-\frac{N_0 L^3}{M_1}\right) \times \sinh\left(\frac{N_0 L^3}{M_1}\left(1 - \frac{M_0}{N_0}\right)^{1/2}\right) \tag{69}$$

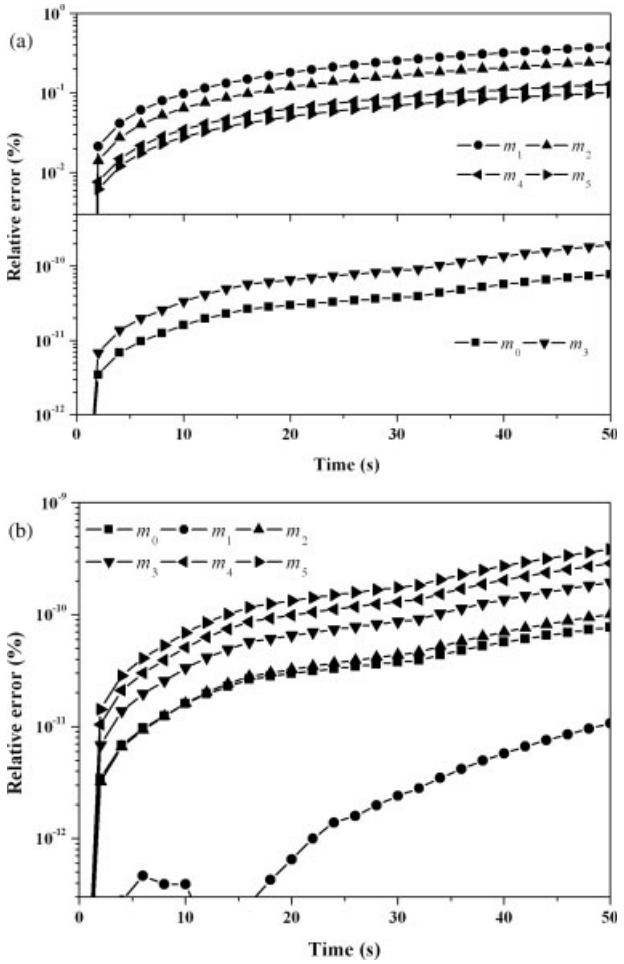

Figure 13. Evolution of percentage errors with time for the first six moments using DQMOM and ADQMOM for aggregation with a constant kernel and growth process with a linear rate together with Gauss-like initial distribution.

"Square": m_0, "Circle": m_1, "Up triangle": m_2, "Down triangle": m_3, "Left triangle": m_4, "Right triangle": m_5. (a) DQMOM and (b) ADQMOM.

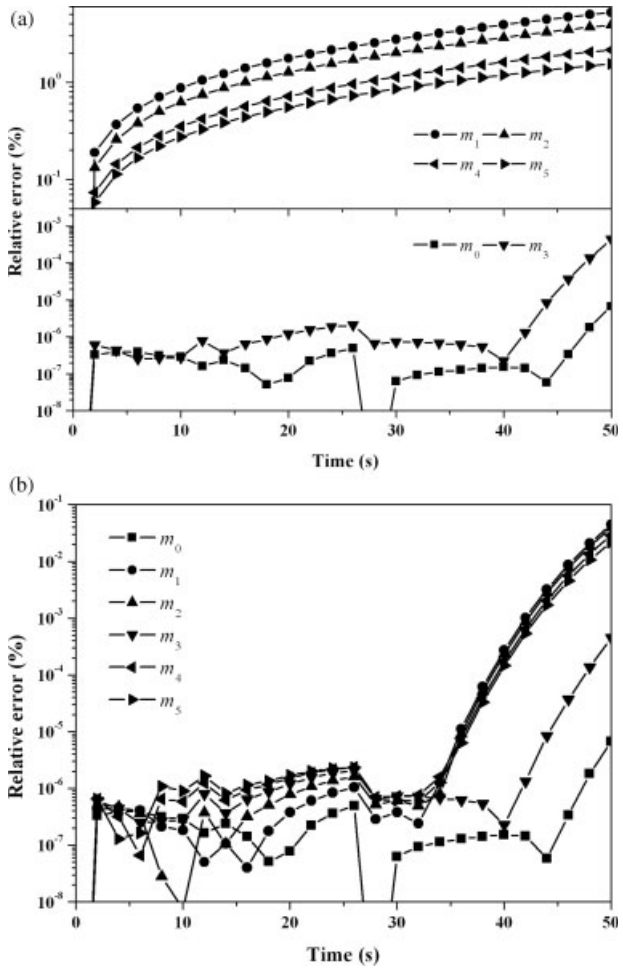

Figure 14. Evolution of percentage errors with time for the first six moments using DQMOM and ADQMOM for aggregation with a sum kernel and growth process with a linear rate together with exponential initial distribution.

"Square": m_0, "Circle": m_1, "Up triangle": m_2, "Down triangle": m_3, "Left triangle": m_4, "Right triangle": m_5. (a) DQMOM and (b) ADQMOM.

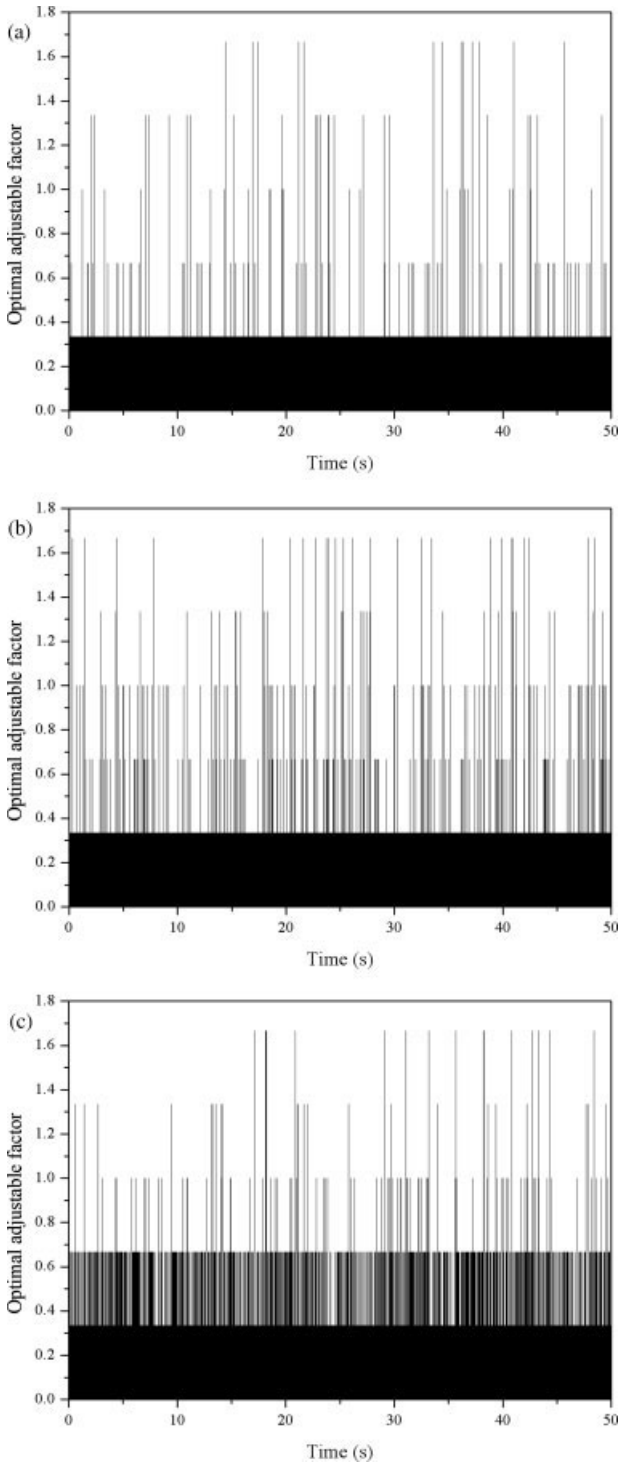

Figure 15. Variation of optimal adjustable factor with time for three different test cases.

(a) the first test case in pure aggregation, (b) the second test case in pure breakage, and (c) the first test case in pure growth.

where $M_0 = 2N_0/(2 + C_0N_0t)$, $M_1 = N_0V_0\exp(G_0t)$. Again, the standard moments were obtained using numerical integration. Results for percentage errors presented in Figure 13 for (a) DQMOM and (b) ADQMOM shows very similar trend to those in the previous test case although a different initial distribution was used, demonstrating that ADQMOM is capable of improving the numerical accuracy greatly at little additional computational cost.

In the last test case, the sum kernel was adopted for aggregation, i.e. Eq. 43 with $C_0 = 0.01$, and a linear rate was used for growth, i.e. Eq. 67 with $G_0 = 0.01$, together with an exponential initial distribution, Eq. 38. In such a situation, the analytical solution for NDF is[20]

$$f(L;t) = \frac{3M_0 \exp[-M_0L^3(2N_0/M_0 - 1)/M_1]I_1(2N_0L^3(1 - M_0/N_0)^{1/2}/M_1)}{L(1 - M_0/N_0)^{1/2}} \tag{70}$$

where,

$$M_0 = N_0 \exp\left[\frac{C_0 N_0 V_0}{G_0}(1 - \exp(G_0 t))\right] \tag{71}$$

and $M_1 = N_0 V_0 \exp(G_0 t)$, $I_1(x)$ is the modified Bessel function of the first kind. Numerical integral was used to evaluate the moments. Percentage errors for all the moments presented in Figure 14 for (a) DQMOM and (b) ADQMOM, show that the maximum error is 5.22% with DQMOM, whereas for ADQMOM all errors are below 0.1% within the simulation time. An obvious feature of Figure 14b is that percentage errors fluctuate when they are low and begin to rise at 32 s for m_1, m_2, m_4, and m_5, and after 40 s for m_0 and m_3. Both the standard DQMOM and our method should have yielded good accuracy for m_3, with percentage errors reaching the computer precision throughout all the simulation time, because mass conservation was considered in the simulation, but there was also a sharp rise. Thus the rise in errors after around 35 s is due to the presence of the Bessel function in NDF and the numerical integration procedure used rather than ADQMOM. The moments cannot be evaluated exactly and if errors from the integration procedure are comparable with those of the numerical method and both are low in magnitude, the relative errors will fluctuate. Since numerical errors for m_1 m_2 m_4, and m_5 with the standard DQMOM are much larger than those of the numerical integration, the same feature cannot be observed in Figure 14a.

Variation of optimal adjustable factor

The procedure for searching the optimal adjustable factor is executed at each time point. To investigate the evolution of the optimal adjustable factor with time, three previously shown test cases were examined, one for each of the three processes: pure aggregation, pure breakage, and pure growth. Figure 15 depicts the variation of optimal adjustable factor with time for (a) the first test case in pure aggregation, (b) the second test case in pure breakage, and (c) the first test case in pure growth. An obvious common feature is that, within the finite range {1/3, 2/3, 1, 4/3, 5/3}, $p = 1/3$ is chosen during most of the simulation time. Especially in the pure aggregation case, the occurrence of $p = 1/3$ exceeds 90%. Similar observation was made with the modified QMOM,[6] which was found to yield the most accurate results with an adjustable factor $p = 1/3$. Comparison of the results from QMOM with $p = 1/3$[6] and those from ADQMOM showed that the numerical accuracy with the new method was improved further. In the other test cases, similar results were obtained, i.e. $p = 1/3$ was most frequently determined to be the optimal adjustable factor. It is worth pointing out that the optimal adjustable factor is problem and distribution dependent. Whether $p = 1/3$ can satisfy the needs of more complex processes and whether other adjustable factors contribute less to reduce error accumulation would require further investigation.

Conclusions

An adaptive DQMOM (ADQMOM) for PBEs is proposed here, by introducing an adjustable factor to the standard DQMOM and a novel procedure for obtaining the optimal adjustable factors. A number of test cases were carried out to validate the method. Our results demonstrate that ADQMOM is capable of achieving much higher accuracy than the standard DQMOM for aggregation processes without incurring additional computational expense, whereas for breakage problems, it is only effective at improving numerical accuracy if a constant kernel is used. For breakage processes with a power kernel, although numerical accuracy is insensitive to the introduction of adjustable factors, ADQMOM is effective at reducing computational time. Moreover, ADQMOM can alleviate problems in some test cases where poor numerical accuracy is due to the standard DQMOM being too sensitive to physical parameters. For growth processes, ADQMOM has further improved the numerical accuracy even though the standard DQMOM is sufficient. The main issue with DQMOM for growth problems is not numerical accuracy but computational time. Our previous study has shown that significant reduction in computational expense can be achieved by introducing adjustable factors to QMOM,[6] hence further work will be carried out in searching for the adjustable factor that is computationally most efficient. For most of the test cases presented here, $p = 1/3$ appears to be the most frequently adopted optimal adjustable factor. Whether DQMOM with $p = 1/3$ can satisfy the needs of more complex processes will require further investigation. The method proposed here can be coupled with CFD codes relatively easily.

Acknowledgments

This study is financially supported by the National Basic Research Program of China (No. 2004CB720208) and the National Natural Science Foundation of China (No. 40675011). The authors also appreciate the support of Key Laboratory of Mechanics on Western Disaster and Environment.

Literature Cited

1. Kumar S, Ramkrishna D. On the solution of population balance equations by discretization. I. A fixed pivot technique. *Chem Eng Sci*. 1996;51:1311–1332.
2. Kumar S, Ramkrishna D. On the solution of population balance equations by discretization. II. A moving pivot technique. *Chem Eng Sci*. 1996;51:1333–1342.
3. Vanni M. Approximate population balance equations for aggregation-breakage processes. *J Colloid Interface Sci*. 2000;221:143–160.
4. Smith M, Matsoukas T. Constant-number Monte Carlo simulation of population balances. *Chem Eng Sci*. 1998;53:1777–1786.
5. Tandon P, Rosner DE. Monte Carlo simulation of particle aggregation and simultaneous restructuring. *J Colloid Interface Sci*. 1999;213:273–286.
6. Su JW, Gu ZL, Li Y, Feng SY, Xu XY. Solution of population balance equation using quadrature method of moments with an adjustable factor. *Chem Eng Sci*. 2007;62:5897–5911.
7. McGraw R. Description of aerosol dynamics by the quadrature method of moments. *Aerosol Sci Technol*. 1997;27:255–265.
8. Rong F, Marchisio D, Fox RO. Application of the direct quadrature method of moments to polydisperse gas solid fluidized beds. *Powder Technol*. 2004;139:7–20.
9. McGraw R, Wright DL. Chemically resolved aerosol dynamics for internal mixtures by the quadrature method of moments. *J Aerosol Sci*. 2003;29:189–209.
10. Marchisio DL, Pikturna JT, Fox RO, Vigil RD, Barresi AA. Quadrature method of moments for population-balance equations. *AIChE J*. 2003;49:1266–1276.
11. Marchisio DL, Vigil RD, Fox RO. Quadrature method of moments for aggregation breakage processes. *J Colloid Interface Sci*. 2003;258:322–334.

12. Wang L, Marchisio DL, Vigil RD, Fox RO. CFD simulation of aggregation and breakage processes in laminar Taylor-Couette flow. *J Colloid Interface Sci*. 2005;282:380–396.
13. Wang L, Vigil RD, Fox RO. CFD simulation of shear-induced aggregation and breakage in turbulent Taylor-Couette flow. *J Colloid Interface Sci*. 2005;285:167–178.
14. Wright DL, McGraw R, Rosner DE. Bivariate extension of the quadrature method of moments for modeling simultaneous coagulation and sintering of particle populations. *J Colloid Interface Sci*. 2001; 236:242–251.
15. Marchisio DL, Fox RO. Solution of population balance equations using the direct quadrature method of moments. *J Aerosol Sci*. 2005;36:43–73.
16. Scott WT. Analytic studies of cloud droplet coalescence I. *J Atmos Sci*. 1968;25:54–65.
17. Smit DJ, Hounslow MJ, Paterson WR. Aggregation and gelation. I. Analytical solutions for CST and batch operation. *Chem Eng Sci*. 1994;49:1025–1035.
18. Ziff RM, McGrady ED. The kinetics of cluster fragmentation and depolymerisation. *J Phys A: Math Gen*. 1985;18:3027–3037.
19. McCoy BJ, Madras G. Analytical solution for a population balance equation with aggregation and fragmentation. *Chem Eng Sci*. 2003; 58:3049–3051.
20. Ramabhadran TE, Peterson TW, Seinfeld JH. Dynamics of aerosol coagulation and condensation. *AIChE J*. 1976;22:840–851.

Manuscript received Oct. 11, 2007, revision received Mar. 1, 2007, and final revision received Jun. 20, 2008.